NON-EQUILIBRIUM SOLIDIFICATION AND MICROSEGREGATION IN CENTRIFUGALLY CAST HIGH SPEED STEEL FOR ROLLS

U. Klančnik [a,*], B. Košec [a], P. Mrvar [b], J. Medved [b]

[a]* Valji, d.o.o., Štore, Slovenia
[b] University of Ljubljana, Faculty of Natural Sciences and Engineering, Department of Materials and
Metallurgy, Ljubljana, Slovenia

Abstract

When regarding as-cast microstructures of highly alloyed metals, microsegregation of alloying elements is a common feature resulting from non-equilibrium conditions during solidification. The aim of this work is to predict the occurrence and severity of microsegregation in highly alloyed, centrifugally cast high speed steel used for rolls. The prediction was performed using thermodynamic Scheil-Gulliver modelling with Thermo-Calc software. The modelled predictions were then compared with differential scanning calorimetry, X-ray diffraction, light and electron microscopy with energy dispersive spectroscopy, all performed on an as-cast roll shell. Results show that chromium, molybdenum and vanadium have the highest tendency to microsegregation. Vanadium tends to form negative microsegregation, while molybdenum and chromium form positive microsegregation. Scanning electron microscopy revealed the presence of complex eutectic carbides, confirming the Scheil-Gulliver non-equilibrium solidification path via two main successive eutectic reactions.

Keywords: Microsegregation; High speed steel; Scheil-Gulliver model; Differential scanning calorimetry

1. Introduction

High speed steels (HSS) are a group of highly alloyed tool steels designed for specific wear resistant applications, mostly at temperatures above 500°C. The application for cutting tools at high speeds gave them their name [1, 2]. An adjusted HSS alloy with a higher carbon amount (> 1.2 wt. %) is commonly used for working layers for rolls used in the first finishing stands of hot strip mills [3, 4]. Many researchers have reported on the microstructural composition of high-carbon HSS alloys as consisting of various eutectic carbides (MC, M_2C, M_6C and M_7C_3) embedded in a martensitic matrix with some retained austenite [3, 5, 6, 7, 8]. The type of eutectic carbides represented in a particular alloy depends on the content and mutual ratio of carbide-forming elements, such as Mo, W, Cr, and V. The overall chemical composition of the HSS alloy has a profound impact on its solidification path. Researchers have thus far reported on the solidification path through different eutectic reactions that follow crystallization of primary austenite; the eutectic reaction L ➔ (γFe + MC) is common to every report due to a high vanadium content, followed by either L ➔ (γFe + M_2C) [6], L ➔ (γFe + M_7C_3) [7] or L ➔ (γFe + M_6C) eutectic reaction [5].

A. Ghosh [9] offers a review on the formation of microsegregation in cast products, where microsegregation is said to stem from freezing of solute enriched liquid in the interdendritic spaces. Different alloying elements have a different tendency towards microsegregation development, depending on their respective partition coefficient, $k = C_S/C_L$, where C_S is the composition of the solid phase, and C_L the composition of the liquid phase. This process is strictly related to non-equilibrium solidification parameters, where complete mixing in the liquid phase and limited diffusion in the already solidified phase is assumed. The degree of microsegregation can be evaluated using the so-called microsegregation ratio, m, which is defined as a ratio between the maximum and the minimum solute concentration through the dendrite or crystal grain cross section [10]:

$$m = \frac{C_{max}}{C_{min}}$$

Gulliver proposed a model incorporating the statement of limited diffusion in solid as a qualitative description [11, summarized in 10, 12]. Some thirty years later, Scheil [13, summarized in 10, 12] provided a mathematical model in the form of a

differential equation:

$$\left(C_L - C_S\right)\delta f_S = \left(1 - f_S\right)\delta C_L$$

where f_S represents the fraction of solid. The model's analytical solution is as follows:

$$C_S = kC_0\left(1 - f_S\right)^{k-1}$$

in which C_0 represents the nominal composition. When regarding diffusion speed of alloying elements in steel, a substantial difference can be assumed between substitutional and interstitial elements (e.g. carbon, nitrogen). It is this back-diffusion of interstitial elements that proved complex when applying analytical solidification models to steel alloys. One such analytical solution was proposed by Brody and Flemings [14] who implemented a back-diffusion parameter as a constant related to the solid diffusivity D_i^S of solute element i. Clyne and Kurz [15] developed the model further, using a function of the back-diffusion parameter, which worked for infinitely fast moving interstitial elements. Other simpler or more complex models have been proposed by Ohnaka [16], Kobayashi [17], and Nastac and Stefanescu [18]. Ultimately, asymptotical values of these modified equations lead to the lever-rule equilibrium model when $D_i^S \to \infty$, or to the Scheil-Guliver (S-G) model when $D_i^S \to 0$ [19].

Researchers proposed an S-G model devised specifically for steel assuming an infinitely fast diffusion of interstitial elements in all phases, while for substitutional elements this is only valid in liquid and ferrite phases [12]. Their experimental validations show that the S-G model is a robust method for modelling the liquid-solid interval during the process of solidification with a satisfactory accuracy in spite of the model's limitations (k and the liquidus slope are considered as straight lines, highly restrictive assumptions regarding diffusion and liquid-solid interface) [20]. Amongst other proposed solidification models [21], it is also the most widely used and incorporated into commercial software for thermodynamic calculation, such as Thermo-Calc [22]. The S-G calculation for non-equilibrium solidification incorporated in Thermo-Calc software in particular results in an estimation of the solidification range of an alloy. The calculation is based on the assumption of a homogeneous liquid phase and zero diffusivity in solid, where the latter assumption can be disregarded for certain selected components, such as carbon [23]. The partition coefficients, although used as a constant or function in the analytical models, can be numerically computed in dependence on temperature and changing composition by using appropriate thermodynamic software and databases [19, 23].

Centrifugal casting is nowadays widely used in the production of rolling mill rolls, continuous casting rollers, bimetallic tubes, special pipelines and so on. The benefits of centrifugal casting include a more finely formed grain structure with good control of non-metallic inclusion content and other casting defects. Typical as-cast microstructures in centrifugally cast castings include a thin chilled layer near the mould interface, followed by a well-oriented columnar microstructure and, finally, where the dendrite arm breakage induces a heterogeneous nucleation during solidification, an equiaxed microstructure towards the middle of the casting wall. These transitions between different microstructures may lead to more or less pronounced microsegregation, whether near the mould interface, or in the central equiaxed grain microstructure [10, 24].

The aim of this research work is to employ S-G model in predicting solidification in the case of centrifugal casting. A model of solute enrichment of the final solidification front is simulated, thus predicting the occurrence of microsegregation in a high alloyed HSS used for rolls. Energy dispersive spectroscopy is used to confirm the computer model similarly to ref. [25] using line analysis. The characteristic of microsegregation in as-cast samples was evaluated using the microsegregation ratio of elements, m and effective partition coefficient, k_{ef}.

2. Materials and methods

Thermodynamic modelling was performed with Thermo-Calc 4.1 software using TCFE7 database. An S-G model of solidification was calculated with a chemical composition of $1.91C - 0.69Si - 0.79Mn - 0.96Ni - 7.86Cr + Mo+W - 3.52V + Nb - 84.27Fe$ (in wt. %). The following phases were regarded as possibly stable: liquid, austenite, MC, M_2C, M_3C, M_6C, M_7C_3, and $M_{23}C_6$. Fast diffusion was taken into account for carbon.

Model verification was performed on an industrial scale centrifugally cast HSS hollow roll shell with the chemical composition as defined above, measured with a spark spectrometer. The outer working layer was centrifugally cast in a preheated steel mould. Casting temperature was set at 1440°C and rotation speed was set at 120 g-units according to the mould dimensions. The cast shell was left inside the mould to cool to room temperature. Static casting of the roll core was omitted to avoid influence on the as-cast microstructure of the working layer. The cylindrical shell had an outer diameter of 700 mm, length of 1925 mm and 47 mm wall thickness. No heat treatment was performed, therefore, the research presented in this work is related entirely to the as-cast structure.

Material for sampling was taken 200 mm from the casting's edge. The material was cut across the entire wall cross section so the thickness of the casting was

preserved. Samples were prepared for different analyses. The observation field of different samples was perpendicular to the outer edge and ranged up to 25 mm in depth (roughly half of the shell wall thickness). This way the impact of unidirectional solidification on microstructure and microsegregation formation was observed. Unpublished research performed on horizontal cylindrical cast shells, where the length of the shell is significantly larger than its diameter, showed negligible discrepancies in chemical composition between top and bottom of the shell. This is mostly due to the fact that the shell was cast in a horizontal centrifugal machine, so element segregation almost never occurs in a horizontal direction under controlled casting conditions.

Firstly, a small cylindrical sample taken 20 mm in depth of the shell wall was prepared for differential scanning calorimetry (DSC): diameter approximately 5 mm and 2 mm in height. DSC analysis was performed with STA 449 C Jupiter apparatus from Netzsch. The test was conducted under inert atmosphere (99.999 % Ar) in a gas flow of 10 ml/min. The test cycle consisted of heating up to 1500°C at 10 K/min without an isotherm holding at peak temperature to prevent element loss and any possible gravitational segregation in liquid. For determination of the characteristic temperatures the alloy was studied under non-equilibrium conditions with a cooling rate of 10 K/min. An empty corundum cup was used as reference with a pre-defined base line to exclude sample holder artefacts.

Secondly, metallographic samples were prepared using standard metallographic techniques of grinding (CarbiMet grinding paper from Buehler: 120, 35, and 18 μm grit size, respectively) and polishing (two synthetic polish cloths from Buehler with 2 μm diamond paste). Samples were etched for optical microscopy: firstly in 2% Nital to reveal the matrix and, after re-polishing, in Groesbeck reagent for colour-etching, thus revealing different types of carbides [26, 27]. Optical microscopy was done on an Olympus BX51M microscope equipped with DP-12 camera.

Next, an examination on polished metallographic samples was done using a scanning electron microscope (SEM) JEOL JSM-5610. Composition control was performed using energy dispersive spectroscopy (EDS) IXRF Systems Inc. The results of the line EDS measurements were additionally processed using Origin software.

Finally, a thin rectangular sample (roughly 20 x 25 mm, taken through the shell wall cross section) was prepared for X-ray diffraction (XRD) analysis to confirm the phase constituents and microstructural composition with the model prediction. Analysis was performed using Phillips PANalytical X'pert PRO diffractometer with a copper cathode under 45 kV and

40 mA. The 2θ diffractogram was recorded between 15 and 90° with a 0.002 °/s recording speed. The lower detection limit for phases was 3 vol. %.

3. Results
3.1. Scheil-Gulliver model

The model for non-equilibrium solidification calculated on the S-G principle is presented in Fig. 1.
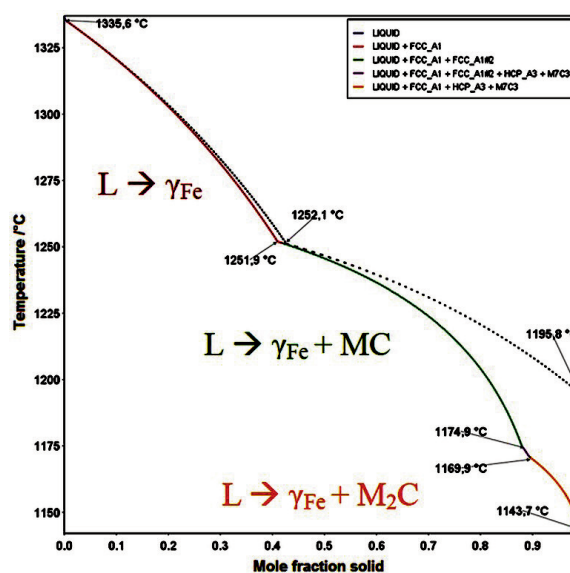

Figure 1. Scheil-Gulliver model for non-equilibrium solidification of the analysed HSS shell, written in simplified form; ferrite suspended. The dashed line represents lever rule equilibrium model

According to the model results, non-equilibrium solidification of the analysed HSS alloy starts at 1335.6°C with crystallization of primary austenite (γFe) from the liquid. A L → (γFe + MC) eutectic reaction follows at 1251.9°C. Between 1174.9°C and 1169.9°C, a short interval with four stable phases is predicted: liquid, austenite, MC, and M_7C_3. In the final step, solidification completes with the additional L → (γFe + M_2C) eutectic reaction at 1143.7°C. Below 1169.9°C the MC phase is presumably not stable according to the computer model.

The dashed line in Fig. 1 represents the lever rule equilibrium solidification model. In contrast to the non-equilibrium S-G model, where a homogeneous liquid phase is assumed along with a limited diffusion in solid (with the exception of carbon), the lever rule equilibrium model assumes a homogeneous composition of all stable phases (unhindered diffusion in solid). This leads to a significant difference in the predicted solidification path. The equilibrium calculation predicts solidification start with austenite (ferrite entered in the calculation) followed by the L → (γFe + MC) eutectic reaction at 1252.1°C.

However, after this reaction, the lever rule model does not predict any other reactions in liquid and solidification completes at 1195.8°C, more than 50°C higher compared to the non-equilibrium model.

Solute enrichment of the remaining liquid during solidification was modelled according to the S-G model. Results are presented in Fig. 2.

The model predicts a steady decrease of Fe in liquid (not shown), which is consistent with crystallization of primary austenite. Fig. 2a shows an increase in elements Mo, Cr and to a lesser extent C. Vanadium in liquid also increases to about 0.4 fraction solid, when the L → (γFe + MC) eutectic reaction takes place. Afterwards its content drops noticeably. Elements Si, Ni, W, and Mn do not show a trend of increase or decrease indicating a constant distribution within the matrix. In the case of Mn, however, a quick increase towards the solidification finish ($f_s > 0.9$) is observed. This predicted phenomenon is a subject of further investigation. Element distribution in austenite (Fig. 2b) shows a very constant content of solute elements up to 0.4 f_s, when V content suddenly drops due to the above mentioned eutectic reaction. This indicates that V should form negative microsegregation along the dendrite cross section. On the other hand, the results for both Mo and Cr in austenite show an increase indicating the formation of positive microsegregation.

3.2. Differential scanning calorimetry

The DSC cooling curve of the analysed HSS working shell sample is presented in Fig. 3. Exothermic peaks that were detected with the DSC analysis are compared to the S-G modelled temperatures to validate the computer model of non-equilibrium solidification (Table 1).
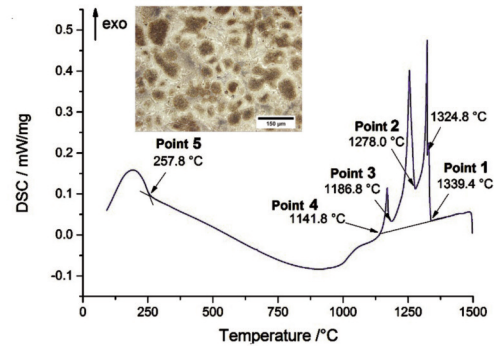
Figure 3. DSC cooling curve of the analysed HSS roll shell (cooling rate was 10 K/min) and an optical microphotograph of the tested DSC specimen, etched in 2% Nital

Table 1. Comparison of phase transformation temperatures during solidification for the analysed HSS roll shell between the DSC measurement and Scheil-Gulliver model

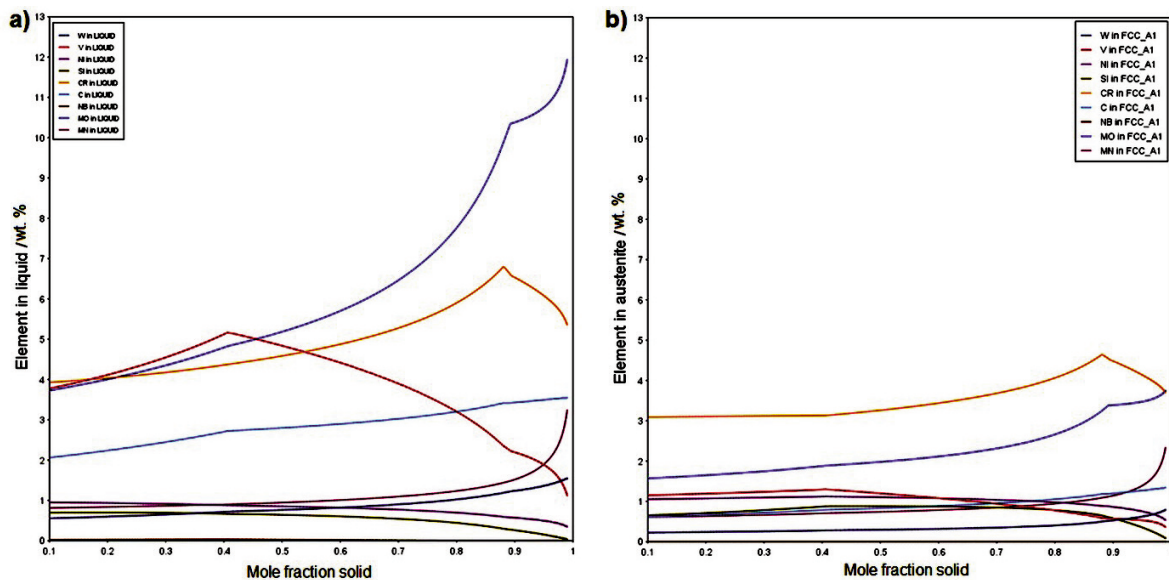| Point	DSC /°C	Scheil-Gulliver model /°C	Phase transformation (simplified)
1	1339.4	1335.6	L → γ_{Fe}
2	1278.0	1251.9	L → (γ_{Fe} + MC)
3	1186.8	1174.9	L → (γ_{Fe} + M$_2$C)
4	1141.8	1143.7	Solidus temperature

Figure 2.   Scheil-Gulliver model results of (a) solute enrichment of the remaining liquid and (b) element composition of austenite, both in relation to fraction solid. Ferrite suspended

Point 5 in Fig. 3 represents the martensite start (Ms) temperature. Experimental and modelled temperatures of phase transformations are in a good agreement. The start and finish temperatures of solidification are accurate within 4°C. The eutectic reactions differ between 10-20°C.

The temperature program of the DSC measurement did not include isothermal holding, especially at maximum temperature (1500°C) and the temperature was kept low enough to prevent any detrimental element loss due to oxidation. Just under the liquidus temperature (at 1324.8°C, marked in Fig. 3), the DSC measurement detected a small deviation inside the larger peak. We attributed this peak to the microsegregation present in the as-cast sample usually observed only as a small change (especially with a larger sample mass). This deviation also coincides well with a correspondent peak seen within the heating curve indicating that microsegregations are present both in the as-cast state and after DSC analysis. This was confirmed further by etching of DSC samples after testing (Fig. 3).

3.3. Optical microscopy and XRD

Phase constitution and composition of the HSS roll shell was confirmed using XRD analysis. Results are presented in Fig. 4.
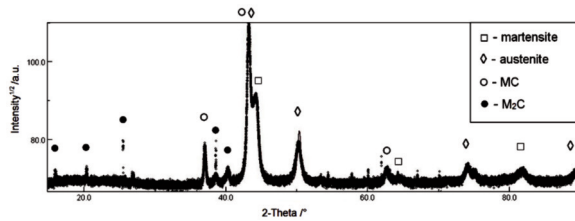

Figure 4. *Results of the XRD analysis of the as-cast sample. M in MC represents elements V and Mo, and in M_2C elements Mo, V, W, Nb. Smaller peaks correspond to non-metallic inclusions (mostly MnS) and are not indexed*

The following phases were detected above their respective detection limit: martensite (34.9 wt. %), austenite (44.4 wt. %), MC carbides with the elements V and Mo (11.2 wt. %) and M_2C with the elements Mo, V, W and Nb (9.0 wt. %). XRD analysis shows a substantial amount of the retained austenite in the as-cast roll shell, due to the high amount of alloying. The S-G model predicts a stable M_7C_3 phase, which was not confirmed with XRD analysis.

Optical microphotographs of the HSS roll shell are gathered in Fig. 5. The etched microstructure reveals a martensitic matrix with a noticeable amount of the retained austenite (marked in Fig. 5c), in agreement with the XRD analysis results. Eutectic carbides form an almost connected carbide network (Figs. 5a, b, and e). A difference between the microstructures at the
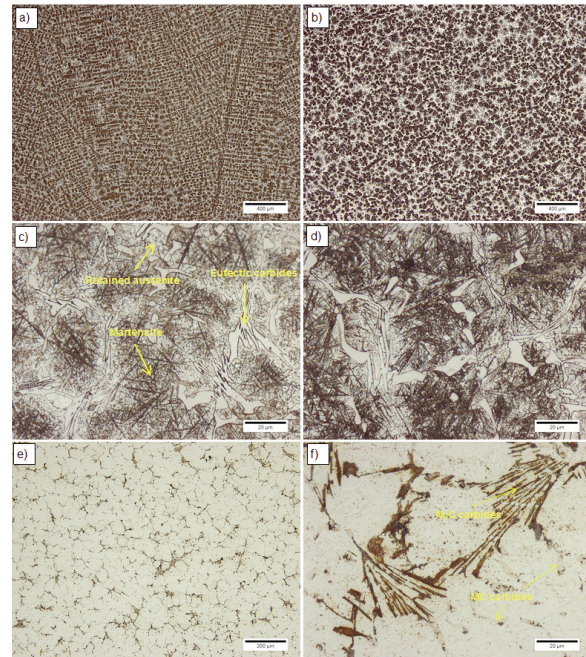

Figure 5. *Optical microphotographs of HSS work shell: (a, c) outer edge of the shell wall and (b, d) 20 mm in depth of the wall. Etched in 2% Nital. (e, f) Colour etched samples 20 mm in depth of the wall, etched in Groesbeck reagent*

outer edge of the shell wall and 20 mm in depth can be seen (Figs. 5a and b). A clearly dendritic microstructure at the outer edge transitions into an equiaxed one in depth. This is the result of various casting parameters such as melt superheat upon pouring, mould temperature and rotation speed, melt modification, substrate surface texture, gas atmosphere, and others [28, 29]. Colour-etching revealed two different types of carbides (Fig. 5f): brown tinted M_2C and smaller, mostly spherical and rod-like MC, shown in light pink with a darker outline.

3.4. Scanning electron microscopy with EDS analysis

Further confirmation of the HSS roll shell phase composition was made with a SEM and EDS analysis. Results are presented in Fig. 6 and Table 2.

SEM microphotographs reveal two distinct carbide phases confirmed with EDS analysis (Table 2):

Table 2. *Results of the point EDS analysis (in wt. %), Figure 6a. The measured carbon is presented informatively*

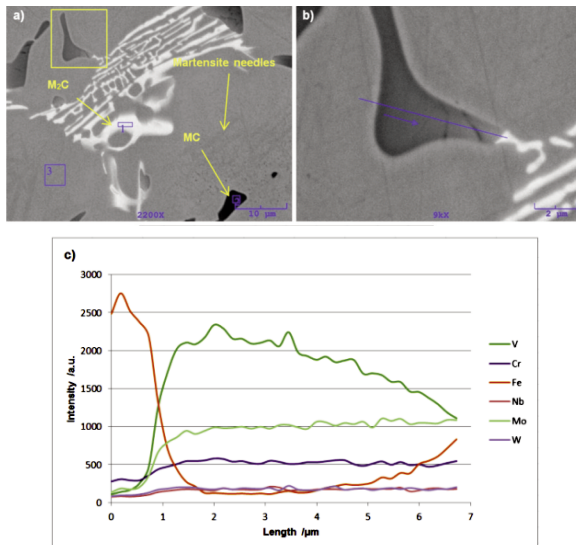|	C	Si	V	Cr	Mn	Fe	Ni	Nb	Mo	W	
1	15.76	-	11.21	16.65	0.61	25.85	0.33	0.45	27.71	1.42	M_2C
2	17.29	0.06	57.09	2.83	0.12	18.71	0.23	0.18	3.12	0.38	MC
3	1.75	1.16	1.23	3.95	0.69	88.43	1.08	0.01	1.54	0.15	Matrix

***Figure 6**. Scanning electron microphotograph of the analysed HSS roll shell with (a) point EDS analysis of the carbides and matrix and (b) line EDS analysis of a complex carbide – marked in (a). (c) Results of the line EDS analysis of the complex carbide*

a light coloured M_2C phase and a darker MC phase, as shown in Fig. 6a. A high carbon value of points 1 and 2 (although not measured quantitatively) indicates that the two analysed phases are indeed carbides as the value of carbon in the matrix is several times smaller. The main constituent of the M_2C phase is Mo, along with a high content of Fe (possibly influenced by the matrix). Cr and V are also present. MC phase revealed V as the main constituent along with Fe and other carbide-forming elements (Mo, Cr, W, and Nb). Nb and W both appear substitutionally dissolved in the carbides, this way improving the carbide's hardness which in turn should improve the wear resistance of the alloy.

The matrix consists mainly of Fe, Si, Mn, and Ni, consistent with the S-G model prediction (Fig. 2b). Due to the high alloying content of carbide-forming elements, some solubility in the matrix is expected. SEM and EDS analysis also did not confirm the phase M_7C_3 that was predicted by the S-G model. The EDS line analysis (Fig. 6b) indicates a transition between one carbide phase and the other, in this case from MC

to M_2C phase. This is consistent with the S-G model in predicting solidification via two main consecutive eutectic reactions.

Further research was done on the presence of microsegregation within the as-cast matrix. Analysis was performed on metallographic samples with line EDS analysis (examples presented in Fig. 7).

The S-G solute enrichment model predicts elements V, Cr, and Mo as most prone to form microsegregation during solidification, so the results presented in Fig. 7 (b, d, f and h) are focused on these three elements. EDS
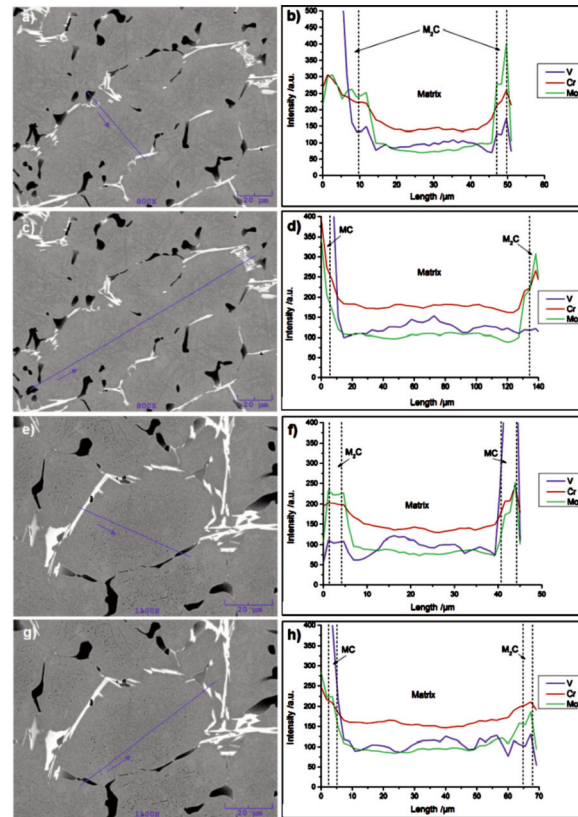

***Figure 7**. Investigation on the presence of microsegregation. Line EDS analysis of a dendrite cross section at the outer edge of the wall shell in (a, b) transverse direction and (c, d) longitudinal direction. Line EDS analysis of a grain cross section, located 20 mm in depth of the wall in (e, f) transverse direction and (g, h) longitudinal direction*

***Table 3.** Results of the calculated microsegregation ratio m and effective partition coefficient k_{ef} for characterization of microsegregation. Measurements were made on the analysed areas shown in Figure 7*

Figure 7	m			k_{ef}		
	V	Cr	Mo	V	Cr	Mo
a	1.36	1.24	1.43	1.37	0.81	0.70
c	1.39	1.02	1.01	1.39	0.98	1.01
e	1.32	1.18	1.25	1.32	0.85	0.80
g	1.27	1.08	1.14	1.27	0.93	0.88
Average	1.34 ± 0.11	1.13 ± 0.16	1.21 ± 0.21	1.34 ± 0.11	0.89 ± 0.14	0.85 ± 0.18

line analysis shows an interesting trend in the distribution of V. Its content decreases from the centre of the grain towards its boundary. On the opposite side, both Mo and Cr increase from the grain centre towards the boundary. The results for the three elements of interest correlate to the calculated model for austenite composition shown in Fig. 2b.

Results of the microsegregation ratio (henceforth abbreviated to ratio) m measured with absolute maximum to minimum ratio on the measured areas in austenite shown in Fig. 7 (presented in Table 3) confirm the formation of microsegregation. The solute concentration, C, was calculated on an average of five adjacent points of the EDS line measurement (presented in Fig. 7). The calculation error was evaluated at 1.5%.

The effective partition coefficient k_{ef} was also calculated from the measured element concentrations as:

$$k_{ef} = \frac{C_{centre}}{C_{edge}}$$

where C_{centre} is the element concentration in the centre of the dendrite/grain ($f_S = 0$) and C_{edge} is the element concentration at the dendrite/grain edge ($f_S = 1$). According to Dubrovská et al. [30], this calculation approach is feasible for the assumption of perfect mixing in the interdendritic area, which is the same basic assumption taken for the S-G model. This way the calculated effective partition coefficient can characterize microsegregation as being negative (element enrichment in the centre of the dendrite/grain, $k_{ef} > 1$) or positive (element enrichment near the edge of the dendrite/grain, $k_{ef} < 1$).

Results in Table 3 show that V has the highest tendency to microsegregate (m). As k_{ef} shows, the microsegregation in this case is indeed negative in contrast to Cr and Mo that form positive microsegregations. Interestingly, the ratio m for V remains constant regardless of the direction of the measurement, whether longitudinal or transverse, dendritic or equiaxed structure. In the case of Cr and Mo, the ratios show a more pronounced microsregregation in the transverse direction (Table 3 a, e) as opposed to the longitudinal direction (Table 3 c, g).

4. Discussion

Results of the investigation reveal a complex, highly alloyed steel alloy with a relatively long solidification interval (~200°C). The solidification path proceeds via crystallization of primary austenite and two main consecutive eutectic reactions correlating to the non-equilibrium solidification path as predicted by the S-G model. No solidification with primary ferrite was detected with thermal analysis and microstructure investigation. It is interesting to note that the equilibrium lever rule solidification model appears considerably different (Fig. 1, dashed line). Also, the measured solidus temperature denoting the finish of solidification is in a good agreement with the S-G model.

All in all, in the case of centrifugally cast hollow roll shell the computed S-G model is sufficiently accurate in spite of its restrictive hypotheses. However not all of the predicted stable phases were confirmed with EDS and XRD methods. Namely, chromium-based M_7C_3 phase, which is first predicted as stable at 1174.9°C, was not detected with the XRD. Either this phase is indeed absent from the alloy (through inhibited precipitation or phase transformation during cooling) or its content does not exceed the XRD detection limit of 3 vol. %.

A high amount of MC and M_2C carbide phases were confirmed with optical microscopy, SEM, EDS, and XRD. One is primarily V-based and the other rich in Mo. Other carbide forming elements represent substitutional elements in the carbides' crystal lattice. These phases precipitate through two main consecutive eutectic reactions thus forming an almost enclosed carbide network as seen in Fig. 5. Crystallization of primary austenite according to the non-equilibrium solidification theory starts with minimal solute elements [20, 31]. The content of solute elements in the solidified austenite slowly increases as solidification progresses. Substitutional solubility of carbide-forming elements in austenite is hindered due to its close packed face cubic centre lattice, so the solute element content increases in the remaining liquid in the inter-dendritic spaces as shown in Fig. 2. Several of Fe-C-M systems, where M represents Cr, V, W etc., exhibit monovariant lines in the form of peritectic or, most often eutectic lines bordering on multiphase areas [20, 31]. As the concentration of carbide-forming elements in the remaining liquid reaches a sufficient composition, precipitation of respective carbide phases begins.

Another important implication of the remaining liquid enrichment on solute, carbide-forming elements is the occurrence of microsegregation. As results show, elements V, Cr, and Mo have the most pronounced tendency towards microsegregation formation. The calculated ratio m (Table 3) revealed V as the most segregated among the three elements. Also, the characteristic of V-based microsegregation is negative, meaning the solute concentration of V in the remaining liquid decreases as solidification progresses. This is due to the eutectic reaction L $\rightarrow$ (γFe + MC) taking place at 0.4 fraction solid, as previous research has shown in a similar high speed steel type cast iron [32]. A similar trend of element solute concentration in the remaining liquid dropping was also predicted in the case of chromium and molybdenum, as the L $\rightarrow$ (γFe + M_2C) eutectic reaction takes place, however, EDS measurements have not confirmed this phenomenon as some diffusion in solid is still present during cooling.

5. Conclusions

Results shown in this study are related to thermodynamic modelling and microsegregation phenomena in high alloyed HSS alloy used for working layers in rolls. The solidification path correlates to the predicted Scheil-Gulliver model and undergoes two main eutectic reactions after primary austenite crystallization:

$L \rightarrow (\gamma Fe + MC)$ and $L \rightarrow (\gamma Fe + M_2C)$. Both V-rich MC and Mo-rich M_2C carbide phases were confirmed using XRD, optical microscopy with sample etching and SEM-EDS analysis. The predicted Cr-based M_7C_3 carbide phase was not confirmed in the sample measurements. Due to the preserved as-cast microstructure, a considerable amount of the retained austenite was found using XRD analysis (44.4 wt. %) occurring near the interdenritic areas, whilst martensite (34.9 wt. %) appears in the dendrite's centres. Line EDS analysis revealed microsegregation of elements V, Cr, and Mo, as predicted with the Scheil-Gulliver model of remaining liquid enrichment. The microsegregation ratio shows the highest tendency to form microsegregation in the case of V, followed by Mo and finally Cr. In contrast to Mo and Cr, which form positive microsegregation (higher solute concentration near the interdendritic areas), V forms negative microsegregation.

References

[1] G. Hoyle, High speed steels, Butterworth, Cambridge, 1988.
[2] G. Roberts, G. Krauss, R. Kennedy, Tool Steels, 5th edition, ASM International, 1998.
[3] Y. Sano, T. Hattori, M. Haga, ISIJ Int., 32 (11) (1992) 1194-1201.
[4] H. Takigawa, T. Tanaka, S. Ohtomo, M. Hashimoto, Nippon steel technical report, 74 (1997).
[5] J. Gontarev, M. Doberšek, J. Medved, P. Mrvar, Metalurgija, 50 (1) (2011) 29-32. .
[6] J. Tchoufang Tchuindjang, M. Sinnaeve, J. Lecomte-Beckers, Proceedings of the 4th International Conference on Abrasion Wear Resistant Alloyed White Cast Iron For Rolling and Pulverizing Mills – Abrasion 2011, August 21-24, Liege, Belgium, 2011, p. 61-75.
[7] M. Pellizzari, MTAEC9, 44 (3) (2010) 121-127.
[8] H. Halfa, JMMCE, 1 (2013) 257-270.
[9] A. Ghosh, Sadhana, 26 (1-2) (2001) 5-24.
[10] A. Royer, S. Vasseur, in ASM Metals Handbook Vol. 15 (D. M. Stefanescu), ASM International, 1990, p. 299-305, 632-640.
[11] G. H. Gulliver, J. Inst. Met. 9 (1913) 120-157.
[12] P. Schaffnit, C. Stallybrass, J. Konrad, F. Stein, M. Weinberg, Calphad, 48 (2015) 184-188.
[13] E. Scheil, Z. Metallkd., 34 (1942) 70-72.
[14] H. D. Brody, M. C. Flemings, Trans. TMS-AIME, 236 (1966) 615-624.
[15] T. W. Clyne, W. Kurz, MTA 12 (1981) 965-971.
[16] I. Ohnaka, Trans. ISIJ 26 (1986) 1045-1051.
[17] S. Kobayashi, Trans. ISIJ 28 (1988) 728-735.
[18] L. Nastac, D. M. Stefanescu, Metall. Trans. A 24A (1993) 2107-2118.
[19] Q. Chen, B. Sundman, Mater. Trans. 43 (2002) 551-559. DOI: 10.2320/matertrans.43.551.
[20] M. Durand-Charre, Microstructure of Steels and Cast Irons, Springer, Germany, 2004, p. 56-95.
[21] M. Trepczyńska-Łent, Archives of Foundry Engineering, 8 (3) (2008) 117-120.
[22] J. O. Andersson, T. Helander, L. Höglund, P. F. Shi, B. Sundman, Calphad, 26 (2002). 273-312.
[23] Thermo-Calc Documentation Set, Thermo-Calc version 2017a (accessed 15 June 2017).
[24] X. Q. Wu, H. M. Jing, Y. G. Zheng, Z. M. Yao, W. Ke, Z. Q. Hu, Mater. Sci. Eng. A, 293 (2000) 252-260.
[25] L. Morales-Rivas, H. Roelofs, S. Hasler, C. Garcia-Mateo, F.G. Caballero, J. Min. Metall. Sect. B-Metall., 51 (1) B (2015) 25-32.
[26] G. Vander Voort, E. Manilova, J. R. Michael, Microscopy and Microanalysis, (Suppl. 02) (2004) 76-77.
[27] J. Lecomte-Beckers, J. Tchoufang Tchuindjang, GIT – Imaging and Microscopy, 2 (2005) 2-3.
[28] U. Klančnik, M. Drobne, B. Košec, P. Mrvar, J. Medved, Proceedings of the 15th International Foundrymen Conference, May 11-13, Opatija, Croatia, 2016, 231-239.
[29] L. Strezov, J. Herbertson, ISIJ Int., 38 (9) (1998) 959-966.
[30] J. Dobrovská, F. Kavička, V. Dobrovská, K. Stránský, H. Francová, MTAEC9 47 (1) (2013), 79-83.
[31] S. Spaić, Physical metallurgy: Composition of metallic materials, Solidification of metal melts, Faculty of Natural Sciences and Technology, Department of Materials and Metallurgy, University of Ljubljana, Ljubljana, 2002 (in Slovenian).
[32] H. Miyahara, S.V. Bravo, K. Yamamoto, K. Ogi, ISIJ Int., 49 (7) (2009) 1075-1079.

NERAVNOTEŽNO OČVRŠĆAVANJE I MIKROSEGREGACIJA KOD CENTRIFUGALNO LIVENOG BRZOREZNOG ČELIKA ZA VALJKE

U. Klančnik [a,*], B. Košec [a], P. Mrvar [b], J. Medved [b]

[a*] Valji, d.o.o., Štore, Slovenija
[b] Univerzitet u Ljubljani, Fakultet prirodnih nauka i inženjerstva, Odsek za materijale i metalurgiju, Ljubljana, Slovenija

Apstrakt

Mikrosegregacija legirajućih elemenata u mikrostrukturi livenih visokolegiranih metala je uobičajeno svojstvo koje je rezultat neravnotežnih uslova tokom njihovog očvršćavanja . Cilj ovog rada je da predvidi učestalost i intenzitet mikrosegregacije u visokolegiranom, centrifugalno izlivenom brzoreznom čeliku koji se koristi za valjke. Predviđanje je izvedeno korišćenjem termodinamičkog Scheil-Gulliver modeliranja, uz pomoć Thermo-Calc softvera. Rezultati predviđanja su upoređeni sa rezultatima diferencijalne skenirajuće kalorimetrije, rentgenske difrakcije, optičke i elektronske mikroskopije sa energetsko disperzivnom spektroskopijom, dobijenih na izlivenom omotaču valjka. Rezultati pokazuju da hrom, molibden i vanadijum imaju najveću tendenciju ka mikrosegregaciji. Vanadijum teži ka formiranju negativne mikrosegregacije, dok molibden i hrom formiraju pozitivne mikrosegregacije. Skenirajuća elektronska mikroskopija je otkrila prisustvo složenih eutektičkih karbida, potvrđujući Scheil-Gulliver putanju neravnotežne solidifikacije pomoću dve glavne sukcesivne eutektičke reakcije.

Ključne reči: Mikrosegregacija; Brzorezni čelik; Scheil-Gulliver model; Diferencijalna skenirajuća kalorimetrija.